New range-based neighbourhood operator for extracting edge and texture information from mammograms for subsequent image segmentation and analysis

R.Chandrasekhar and Y.Attikiouzel

Abstract: A new, spatially isotropic, range-based, neighbourhood operator is described, and its use for extracting edge and texture information from mammograms is illustrated. It is an extension of an operator, first introduced by J.C. Russ, and founded on the work of H.E. Hurst. An octagonal neighbourhood is defined, centred on each pixel in an image, and the difference between the maximum and minimum pixel values in each set of pixels at a given Euclidean distance from the centre pixel is computed to be the range. The logarithm of the range is plotted against the logarithm of the distance, and a straight line fitted to the data. The y-axis intercept c and the square of the correlation coefficient, η^2, are associated with the position of the centre pixel. Preliminary experiments suggest that c is edge-sensitive and could be useful in detecting weak edges, with good noise immunity, while η^2 is a promising texture measure that may be used to detect the edge of the pectoral muscle, define the boundary of the mammographic parenchyma, and in conjunction with other features, possibly detect circumscribed lesions.

1 Introduction

Image analysis consists of feature extraction, segmentation and classification [1]. The choice of features is largely experience-driven, while segmentation is really pixel classification [2] and may be pixel-, edge- or region-based. This paper is concerned with detecting image edges and characterising texture as features for edge- and region-based segmentation and analysis of mammograms.

In greyscale images, edges are characterised by abrupt discontinuities in grey-level intensities, and represent object boundaries that are visually apparent. Edges are usually detected by one of three methods: direction-sensitive, mask-based gradient operators like the Sobel operator, which are sensitive to noise; edge detectors using Gaussian-smoothing for better noise immunity, like the Marr–Hildreth operator (or Laplacian of a Gaussian); and the popular Canny operator [3].

Image texture is easily perceived and intuitively understood. It is, however, difficult to characterise mathematically with sufficient generality to encapsulate the whole gamut of perceived textures. Multi-pronged approaches to texture description and analysis have therefore been developed [1, 4]. One of these is to classify textures as strongly ordered, weakly ordered and disordered, with the observation that these textures could best be described using structural, oriented-flow, and statistical/fractal descriptors respectively [5].

IEE Proceedings online no. 20000853

DOI: 10.1049/ip-smt:20000853

Paper first received 7th June and in revised form 30th August 2000

The authors are with the Australian Research Centre for Medical Engineering, The University of Western Australia, Nedlands, WA 6907, Australia

We present here a new range-based neighbourhood operator, extending from the work of J.C. Russ [6], that, in one operation extracts both edge and texture information from an image, and apply it to mammogram edge detection and texture analysis, as part of the global segmentation of mammograms. It is based on a statistical quantity: the range of greyscale values in successive, equidistant 'annuli' around a centre pixel.

The operator yields two new parameters: one that emphasises edges and another that is texture-sensitive. The edge measure is suited to defining relatively strong edges of variable absolute strength like the skin line on a mammogram. The texture measure very likely captures fractal and/or statistical behaviour and appears well-suited to characterising mammogram texture, which lies somewhere in the texture spectrum between a weakly ordered and a disordered texture.

2 The Russ operator

In 1990, J.C. Russ [6] introduced a 'local Hurst operator' to perform texture discrimination. He claimed that this operator implemented in two dimensions the method that H.E. Hurst [7] had introduced in studying time-series related to river flow data. While it has been shown elsewhere [8] that Russ's implementation differs from Hurst's in five ways, the operator introduced by Russ is nevertheless very interesting and useful in its own right, and is called the Russ operator in this paper.

Mandelbrot and co-workers [9–11] introduced the fractional Brownian motion (FBM) model to account for the behaviour extracted by Hurst's method, although it is not known at present whether this is the only applicable model. Moreover, it is unclear whether FBM is a valid model for explaining what the Russ operator does, given its departures from Hurst's method.

The Russ operator [6] is most easily understood with an example. An octagonal neighbourhood of given radius ρ is first defined for any particular pixel in an image. For example, the neighbourhood shown in Fig. 1 is defined for a radius of four or a diameter of nine pixels; the centre pixel is labelled 0. This neighbourhood is an approximation to a circle, which is the equidistant locus in the Euclidean norm. The distances associated with each labelled pixel in Fig. 1 are shown in Table 1.

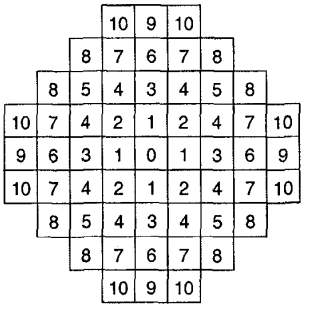

Fig. 1 *Octagonal neighbourhood of radius $\rho = 4$ and diameter 9*
Pixels at the same Euclidean distance d_k from the central pixel, numbered 0 above, are labelled with the same index, k. See Table 1 for the relevant distances

Table 1: Label-distance table for octagonal neighbourhood

Pixel label k	No. of pixels	Euclidean distance d_k
0	1	0
1	4	1
2	4	$\sqrt{2}$
3	4	2
4	8	$\sqrt{5}$
5	4	$2\sqrt{2}$
6	4	3
7	8	$\sqrt{10}$
8	8	$\sqrt{13}$
9	4	4
10	8	$\sqrt{17}$

Showing Euclidean distances d_k corresponding to the indices k shown on the octagonal neighbourhood of radius $\rho = 4$ in Fig. 1

For a given radius ρ and centre pixel $\boldsymbol{p}$ in a greyscale image, Russ defined his 'local Hurst operator' so:

1. For each set of pixels lying within the neighbourhood, at the same Euclidean distance d from the centre pixel, find the maximum and the minimum pixel values. Their difference is the range, R.

2. Plot log R against log d and fit a straight line to the data to minimise the square of the error.

3. The slope of the plot m is a measure of 'local roughness (in the sense of the Hurst coefficient)' [6] at the centre pixel. It could be used to plot a transformed image, scaled for display, that could later be segmented on the basis of the m values.

As an example, Fig. 2 shows a sample plot for a single centre pixel position on an image, with $\rho = 4$. There are 10 points on the plot (corresponding to the 10 different distances from the centre pixel in Table 1) and the degree of fit to the straight line is good, as exemplified by the square of the coefficient of correlation, which at 0.975 is very close to 1.

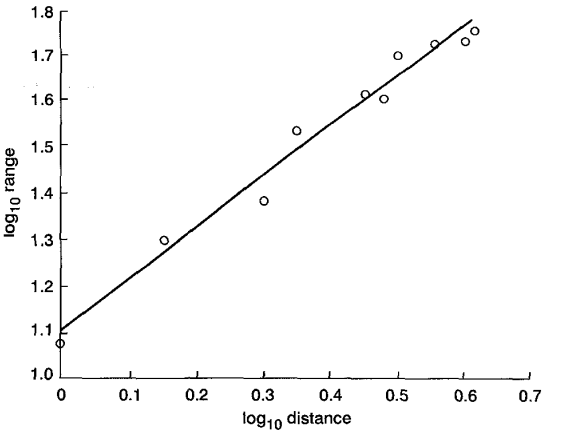

Fig. 2 *Straight line fitted to the 10 points arising from the neighbourhood of radius $\rho = 4$*
The centre pixel has co-ordinates (171, 467), at 400μm per pixel, for MIAS mammogram image mdb005ll. The values of (m, c, η^2) are (1.09, 1.10, 0.975)

Russ interpreted his results in light of the FBM model, claiming that '... the slope of the resulting line is directly related to the fractal dimension of the profile' [6]. He therefore used only one parameter, the slope m of the plot.

3 Extended Russ operator

By interpreting the Russ operator purely as a data analysis method, we may extract two more parameters from the process of fitting a straight line. These are:

1. the y-axis intercept, c, and

2. the square of the coefficient of correlation η^2, resulting from the straight line fit.

We define the extended Russ operator $\mathcal{E}$ so:

$$\mathcal{E}(\rho, \boldsymbol{p}) = \begin{pmatrix} m \\ c \\ \eta^2 \end{pmatrix}_{\boldsymbol{p}} \tag{1}$$

where ρ is the radius of the associated octagonal neighbourhood, and $\boldsymbol{p}$ the position of the centre pixel. The output vector has three components: m, c and η^2, which correspond respectively to the slope, y-axis intercept and square of the coefficient of correlation. This vector is associated with $\boldsymbol{p}$.

To avoid edge effects, only those pixels whose neighbourhoods lie wholly within the image are transformed. Also, to avoid undefined values, whenever R is equal to 0, it is (arbitrarily but consistently) set to 1. We note in passing that we have used log to mean $\log_{10}$ while Russ defined it to be ln.

Russ [6] scaled the m-values associated with each pixel position and displayed them as images. We do the same with the c- and η^2-values.

4 Results with mammograms

The extended Russ operator was applied to digitised mammograms from the MIAS database [12], low-pass filtered and reduced in resolution to 400μm per pixel in the x and y directions, with a bit-depth of 8.

4.1 m-, c- and η^2-images for $\rho = 3$

In Fig. 3*a* we show an original mammogram, mdb009ll, from the MIAS database. Figs. 4*a*, 5*a* and 6*a* show the three transformed images resulting from our definition of the extended Russ operator. The c-image clearly emphasises edges [13] while the m- and η^2-images exhibit similari-

ties as well as differences, and seem to be sensitive to intensity and texture.

The intensity histograms of the original, m-, c- and η^2-images are shown in Figs. 3*b*, 4*b*, 5*b* and 6*b*, respectively. They appear markedly different, confirming that the three components are extracting information that is independent and possibly different in each case.

4.2 Comparison of the c-image with conventional edge images

We compare the c-image with those from two conventional edge detectors: the Canny edge detector and a window-based edge detector, using the range as an edge feature.

Fig. 7*a* shows the original MIAS mammogram, mdb024rl. The result of passing the original image through

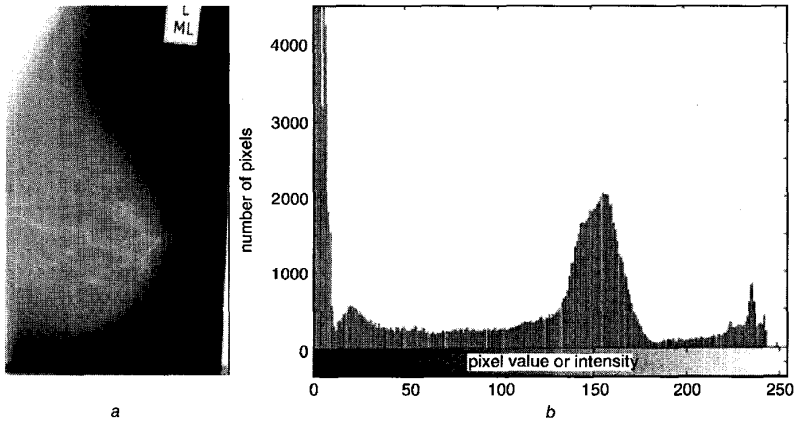

Fig. 3 *Images from extended Russ operator with $\rho = 3$*
a Original image is MIAS mammogram mdb009ll
b Intensity histogram of original mammogram at 400μm per pixel

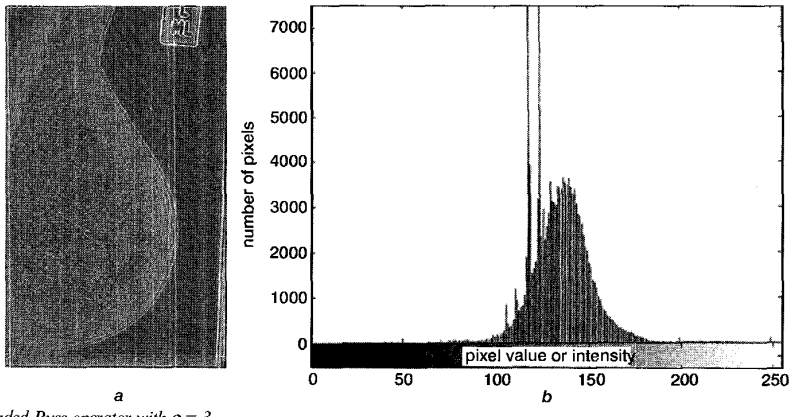

Fig. 4 *Images from extended Russ operator with $\rho = 3$*
a m-image, or 'image of slope values', scaled for display
This results from the original definition by Russ [6], with $\rho = 3$
b Intensity histogram of the m-image from the extended Russ operator
The large spikes on the histogram are associated with the background region

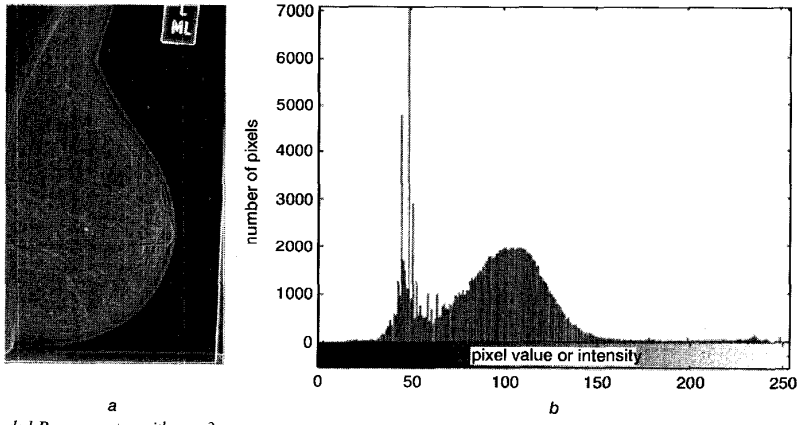

Fig. 5 *Images from extended Russ operator with $\rho = 3$*
a c-image, or 'image of y-axis intercept values', scaled for display
Note the edge sensitivity of the c-component [13]
b Intensity histogram of the c-image from the extended Russ operator
The large spikes on the histogram are associated with the background region

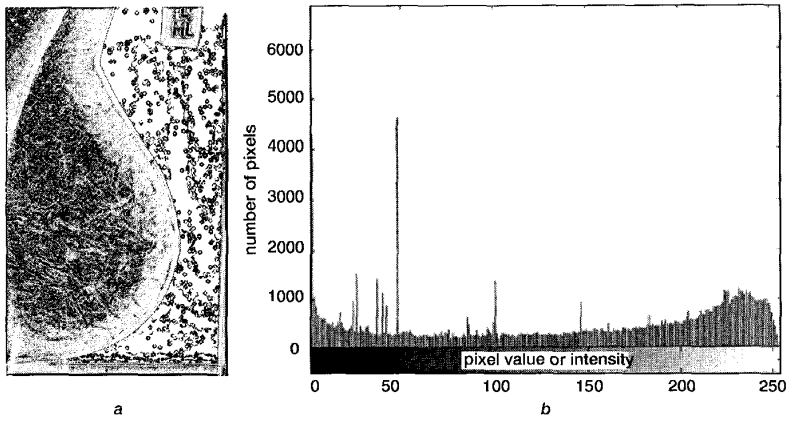

Fig. 6 *Images from extended Russ operator with $\rho = 3$*
a η^2-image, or image of 'the square of the coefficients of correlation', scaled for display
Note the similarities and differences with Fig. 4*a*
Because η^2 has a fixed range of values (from 0 to 1) it may be better suited to extract calibrated texture information
b Intensity histogram of the η^2-image from the extended Russ operator
The large spikes on the histogram are associated with the background region

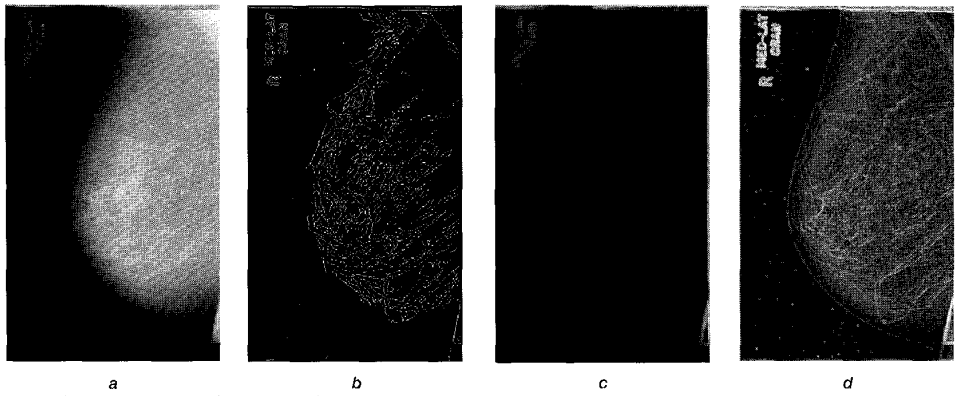

Fig. 7 *Comparison of conventional and c edge images with $\rho = 3$*
a The original mammogram is MIAS image mdb024rl
b Binary Canny edge image from original mammogram
It is not possible to identify an edge corresponding to the skin line
c Scaled image resulting from taking the range within a 7×7 neighbourhood around a pixel in the original image
The skin line is not visible, and details within the breast region are poorly defined
d *c*-component image from the extended Russ operator
The skin line is clearly outlined. This is an analogue edge image in which the edge strength is shown in greyscale

a Canny edge detector is shown in Fig. 7*b*. Although it has picked up many edges, this binary image is unsuitable for detecting the skin line, which does not appear as an edge even partially.

We have shown elsewhere [14] that the range within the neighbourhood of a pixel is a good edge feature. The image in Fig. 7*c* shows the edge image resulting from computing the range of pixel values (difference between maximum and minimum) within a 7×7 neighbourhood centred on each pixel, and scaling and displaying the resulting image. While the strong edges associated with the label are clearly visible, detail within the breast is poor and the skin line cannot be seen.

The *c*-image from the extended Russ operator is shown in Fig. 7*d*. This is an analogue edge image showing edge strength in greyscale, just like Fig. 7*c*. The skin line is clearly outlined from top to bottom. There is also considerable edge detail within the breast, signifying good dynamic range. Notice the vastly different appearance of the images in Figs. 7*c* and *d* although both have used the range in pixel neighbourhoods albeit in quite different ways.

4.3 Comparison of the η^2 and window-based standard deviation images

The results from the η^2-image are now compared with those from a simple, conventional texture measure: the standard deviation of pixel values within a window centred on a pixel.

Fig. 8*a* shows the original MIAS mammogram mdb005ll. The pectoral muscle is the triangular region of higher intensity at the top left of the image. There are two circularly shaped circumscribed mass lesions close to each other, appearing like a figure-of-eight at the lower middle of the image. These are shown in detail in Fig. 8*b*. There is a smaller elliptical opacity in Fig. 8*a*, centred at (176, 297), slightly south-east of the image centre, which is not remarked upon in the MIAS database. A close-up view of this feature is shown in Fig. 8*c*.

The image in Fig. 8*d* is the scaled version of the standard deviation of pixel values within a 7×7 neighbourhood centred on image pixels. The size of this neighbourhood was chosen to correspond roughly to the neighbourhood for the extended Russ operator with $\rho = 3$. The label shows up strongly but the lesions are only faintly outlined. Detailed views corresponding to the regions-of-interest (ROIs) in Figs. 8*b* and *c* are shown in Figs. 8*e* and *f*, respectively.

The η^2-image, shown in Fig. 8*g* is much clearer and shows a light elliptical region with a darker core at the site

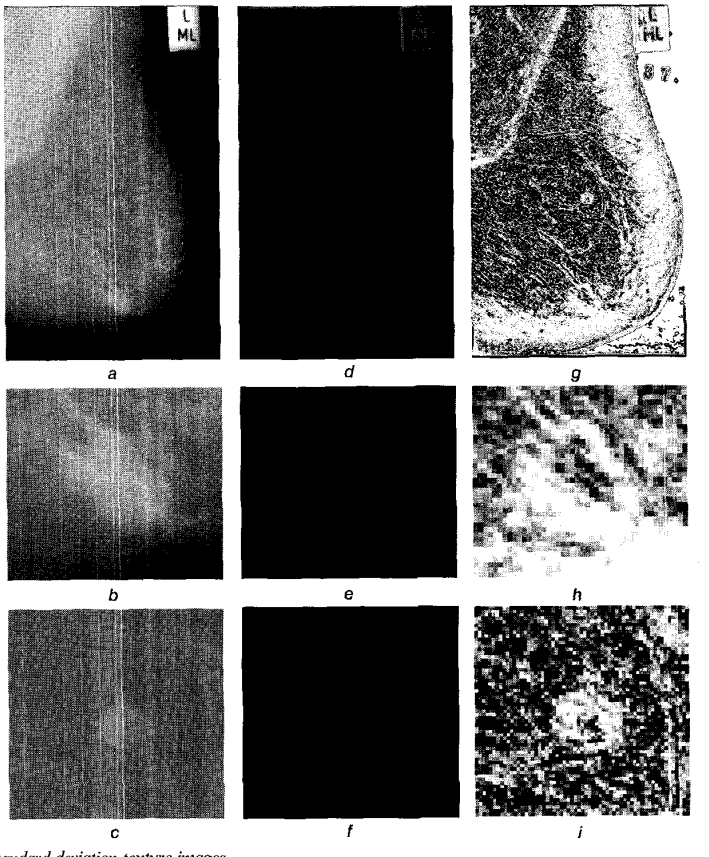

Fig. 8 *Comparison of η^2 and standard deviation texture images*
a Original mammogram is MIAS image mdb005ll
The pectoral muscle appears as a higher intensity triangle at the top left and has a somewhat diffuse border. There are two closely spaced circular lesions of higher intensity, arranged like an oblique figure-of-eight, in the lower middle of the mammogram. There is also a small elliptical opacity in the original image, centred at (176, 297), slightly south-east of the image centre, which is not remarked upon in the database
b Magnification of circular lesions
c Detailed view of elliptical opacity
d Scaled image of the standard deviation of pixel values in a 7 × 7 neighbourhood around each pixel in *a*
The strong edges associated with the label are clear but detail is poor within the breast region, although the lesions are faintly outlined
e Magnified view of circular lesions
f Magnified view of elliptical opacity
g η^2-image of the mammogram for $\rho = 3$, scaled for display
The pectoral muscle edge is predominantly whiter than either the parenchyma to the right, or the rest of the muscle to the left. The subcutaneous fatty region also appears lighter
h A white elliptical region with a black core marks the figure-of-eight lesion site on the η^2-image
i Elliptical opacity is emphasised in the η^2-image as a small, lighter ellipse with a dark spot at the centre

corresponding to the lesion, shown magnified in Fig. 8*h*. The opacity in Fig. 8*c* is also clearly emphasised in the η^2-image as a small, lighter ellipse with a dark spot at the centre, shown in Fig. 8*i*. The pectoral muscle edge and the predominantly fatty subcutaneous region both appear greyish white, while the parenchyma appears black mottled with grey. In each case, the lighter regions on the η^2-image correspond with visually apparent texture boundaries.

5 Discussion

5.1 Qualitative observations

The question may arise as to whether the *c*- and η^2-components of the extended Russ operator are not really capturing the same information as the *m*-component of the original Russ operator. The fact that the intensity histograms in Figs. 4*b*, 5*b* and 6*b* represent different pixel intensity distributions, and are not scaled versions of each other, confirms that we are indeed extracting independent information from the two new components, *c* and η^2, of the extended Russ operator. It is also reasonable to infer that *c* is strongly indicative of edges, whereas *m* and η^2 seem to be correlated with local intensity and visual texture.

5.2 The c-component

It is obvious from Figs. 5 and 7 that the *c*-component of $\mathcal{E}$ emphasises edges. From Fig. 7, it also appears to have a larger dynamic range than either the Canny or the window-based edge detectors.

We speculate that the data fitting in the least squares sense performed by $\mathcal{E}$ confers on the *c*-image some noise insensitivity and a unique ability to detect the relatively strong edges within the neighbourhood, regardless of their absolute strengths. This property should prove useful with medical images where biological variability and imaging technique often result in a single anatomical edge having varying strength along its extent. One important difference between the *c*-component and conventional gradient-based edge detectors is that it is spatially isotropic, and does not embody information on edge direction.

There is also a very high degree of edge detail in the breast region and some form of 'edge spectrum' may need to be developed from the histogram of the *c*-image and used to sort the edges in this region before they may be used, for example, for lesion segmentation.

5.3 The η^2-component

In our opinion, η^2 as a local texture measure has the

advantage of spanning a pre-defined range of values, lying between zero and one, and may therefore be used quantitatively as a calibrated measure.

When the η^2-component is used to analyse mammograms, we have observed the following:

(i) it can clearly outline the skin line;

(ii) the dark, predominantly fatty, region close to the breast border on the original mammogram appears as a predominantly lighter band on the η^2-image, especially for larger ρ;

(iii) the fibroglandular mammographic parenchyma appear as a predominantly dark region which may have patches of lighter regions on it;

(iv) clearly discernible lesions show up as lighter regions (sometimes having a darker core) in the midst of the parenchyma;

(v) the edge of the pectoral muscle shows up as a characteristically lighter band adjoining the darker parenchymal region;

(vi) the mottled appearance of the mammogram background (non-breast region) in the η^2-image indicates that it is highly non-uniform. The 'patches' on the η^2-image, when magnified, may be identified with the shape of the octagonal neighbourhoods used in the operator.

Further experiments with a large number of mammograms are needed to confirm these behaviours generally, and to establish the use of the η^2-component as a reliable texture measure for analysing mammograms. Additional experiments are also required to identify the theoretical basis of the operator, determine what post-processing is needed for texture analysis and segmentation, compare its performance with other texture operators, and explore scale dependence and the possibility of defining a 'texture spectrum'.

5.4 Theoretical ramifications

The straight line fit performed by the extended Russ operator imposes the relationship

$$\log R = m \log d + c \tag{2}$$

which in turn implies the power law relationship

$$R = (10^c) d^m \tag{3}$$

i.e. the range at successive equidistant annuli from the centre pixel increases as the mth power of distance from the centre pixel. While this statement describes the observed behaviour, it does not yield insight into the class of underlying pixel distributions that could lead to this behaviour.

The y-axis intercept of the fitted straight line occurs for $\log d = 0$ which is at unit distance from the centre pixel. A large value for this intercept means that $\log R$ is large, i.e. the range at unit distance from the centre pixel is large at an edge. While this is consistent with the behaviour of range as an edge feature [14], it does not fully explain the observed behaviour, such as why the images in Figs. 7*c* and *d* are so different.

If one assumes that the power law behaviour in eqn. 2 is characteristic of fractals, then, the degree to which the straight line fits the data may indicate the 'degree of fractality' in the neighbourhood of any pixel.

The square of the coefficient of correlation η^2 by definition, lies between zero and one. It may therefore be used as a calibrated, absolute measure of the degree to which the power law behaviour, being tested for by the extended Russ operator, is indeed obeyed. Values close to one signify power law behaviour; values close to zero do not.

We may then conjecture that by setting a threshold for η^2 close to one, and thresholding the image, we may be segmenting those portions of the image that exhibit fractal characteristics, from those that do not.

6 Conclusions

We have defined the extended Russ operator $\mathcal{E}$ as one that maps an octagonal neighbourhood of a pixel to three components, m, c, and η^2, each of which may be scaled and plotted as images. Although computationally intensive, this operator is economical in that both edge and texture information are extracted from an image in a single operation. The c-component may be used to emphasise and detect edges such as the skin line on mammograms. The η^2-component seems to discriminate textures. Because it always takes values between zero and one, it may find use as a calibrated texture measure. Preliminary experiments have revealed that it may be used to define the mammographic parenchyma and the pectoral muscle edge. We conjecture that it may also be capable of highlighting circumscribed masses, very likely in conjunction with other features. Further investigation of the theoretical basis for both the edge detection and texture characterisation is required to understand the relative strengths and weaknesses of the new operator.

7 Acknowledgments

This work was supported in part by an Australian Research Council (ARC) Large Grant.

8 References

1 JAIN, A.K.: 'Fundamentals of digital image processing' (Prentice-Hall, Englewood Cliffs, NJ, USA, 1989), Information and System Sciences Series, p. 343
2 ROSENFELD, A., and KAK, A.C.: 'Digital picture processing' (Academic Press, New York, 1982, 2nd edn.), vol.2, p. 87
3 NALWA, V.S.: 'A guided tour of computer vision' (Addison-Wesley, Reading, MA, USA, 1993)
4 HARALICK, R.M.: 'Statistical and structural approaches to texture', *Proc. IEEE,* 1979, **67**, pp. 786–804
5 RAO, A.R.: 'A taxonomy for texture description and identification' (Springer-Verlag, New York, 1990), Springer Series in Perception Engineering
6 RUSS, J.C.: 'Processing images with a local Hurst operator to reveal textural differences', *J. Comput. Assist. Microsc.,* 1990, **2**, (4), pp. 249–257
7 HURST, H.E., BLACK, R.P., and SIMAIKA, Y.M.: 'Long-term storage: an experimental study' (Constable & Co. Ltd., London, UK, 1965)
8 CHANDRASEKHAR, R.: 'Systematic segmentation of mammograms'. PhD Thesis, Centre for Intelligent Information Processing Systems, Department of Electrical and Electronic Engineering, The University of Western Australia, Nedlands, WA 6907, Australia, October 1996, Chap. 9
9 MANDELBROT, B.B., and VAN NESS, J.W.: 'Fractional Brownian motions, fractional noises and applications', *SIAM Rev.,* 1968, **10**, pp. 422–437
10 MANDELBROT, B.B., and WALLIS, J.R.: 'Noah, Joseph, and operational hydrology', *Water Resources Res.,* 1968, **4**, pp. 909–918
11 MANDELBROT, B.B., and WALLIS, J.R.: 'Robustness of rescaled range R/S in the measurement of noncyclic long run statistical dependence', *Water Resources Res.,* 1969, **5**, pp. 967–988
12 SUCKLING, J., PARKER, J., DANCE, D.R., ASTLEY, S., HUTT, I., BOGGIS, C.R.M., RICKETTS, I., STAMATAKIS, E., CERNEAZ, N., KOK, S.-L., TAYLOR, P., BETAL, D., and SAVAGE, J.: 'The Mammographic Image Analysis Society digital mammogram database' *in* GALE, A.G., ASTLEY, S.M., DANCE, D.R., and CAIRNS, A.Y. (Eds.): 'Digital mammography' (Elsevier Science, Amsterdam, The Netherlands, 1994), Excerpta Medica International Congress Series, vol. 1069, pp.375–378
13 CHANDRASEKHAR, R., and ATTIKIOUZEL, Y.: 'A new edge detector based on the extended Russ operator and its application to mammogram segmentation' *in* MASTORAKIS, N.E. (Ed.): 'Recent advances in signal processing and communications' (World Scientific and Engineering Society Press, Athens, Greece, 1999), pp. 190–193
14 BEZDEK, J.C., CHANDRASEKHAR, R., and ATTIKIOUZEL, Y.: 'A geometric approach to edge detection', *IEEE Trans. Fuzzy Syst.,* 1998, **6**, pp. 52–75